Accepted Manuscript

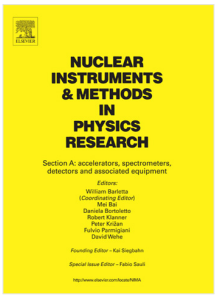

Inner shell ionization of argon in ECRIS plasma

M. Sakildien, R. Kronholm, O. Tarvainen, T. Kalvas, P. Jones, R. Thomae, H. Koivisto

PII: S0168-9002(18)30660-0
DOI: https://doi.org/10.1016/j.nima.2018.05.045
Reference: NIMA 60829

To appear in: *Nuclear Inst. and Methods in Physics Research, A*

Received date : 7 September 2017
Revised date : 2 February 2018
Accepted date : 22 May 2018

Please cite this article as: M. Sakildien, R. Kronholm, O. Tarvainen, T. Kalvas, P. Jones, R. Thomae, H. Koivisto, Inner shell ionization of argon in ECRIS plasma, *Nuclear Inst. and Methods in Physics Research, A* (2018), https://doi.org/10.1016/j.nima.2018.05.045

Inner shell ionization of argon in ECRIS plasma

M Sakildien[1,2], R Kronholm[2], O Tarvainen[1], T Kalvas[2], P Jones[1], R Thomae[1] and H Koivisto[2]

[1] *iThemba LABS (Laboratory for Accelerator Based Sciences), PO Box 722, Somerset West, 7192, South Africa*

[2] *University of Jyväskylä, Department of Physics, 40500 Jyväskylä, Finland*

Abstract

The volumetric $K\alpha$ emission rate of argon emitted from the electron cyclotron resonance (ECR) heated plasmas of the JYFL (University of Jyväskylä, Department of Physics) 14 GHz ECR ion source (ECRIS) and the 14.5 GHz Grenoble Test Source (GTS) at iThemba Laboratory for Accelerator Based Sciences have been measured to gain an understanding of the influence of the ion source tune parameters on the absolute inner shell ionization rate. It was observed that the behaviour of the ionization rate and the extracted ion beam currents react differently, depending the parametric sweep performed. The neutral gas pressure and incident microwave power was found to have the strongest influence on the ionization rate. At high neutral gas pressure, the absolute inner shell ionization rate was found to saturate. This observation is as a result of the plasma energy content becoming insufficient to sustain the growth in ionization rate. It was also observed that the incident microwave power should be increased much more to counter the decrease in high charge state production as a result of the gas increase and subsequent increase in charge exchange. At low incident microwave, the ionization rate per unit absorbed microwave power was found to be high, which suggests that the inner shell ionization process is driven by the ion dynamics as opposed to the electron dynamics. The influence of the biased disc voltage and magnetic field configuration on the ionization rate was found to be minimal. This led to the suggestion that these two tune parameters does not directly impact the warm electron population of the ECRIS plasma during

Preprint submitted to Nuclear Instruments and Methods in Physics Research, AFebruary 2, 2018

the parametric sweeps. The $K\alpha$ emission rate can be used as an additional tool for benchmarking the results of numerical simulation codes on ECRIS plasmas.

Keywords: ECRIS, plasma, volumetric emission rate, inner shell ionization rate

1. Introduction

. Electron cyclotron resonance ion sources (ECRISs) are used to produce multiply charged ions, which are frequently further accelerated and transported, via a transfer beamline, to a target station. To produce multiply charged ions in an ECRIS, plasma electrons are confined by a complex magnetic field, consisting of a solenoidal mirror field and a multipolar field. The vector sum of these two fields is a minimum in the centre of the magnetic field configuration, forming the so-called minimum-B field[1]. As a result of the imposed magnetic field, the plasma electrons spiral around the magnetic flux lines at the cyclotron frequency. To sustain the ECRIS plasma, high-frequency electromagnetic (EM) waves are launched into the plasma chamber from the high magnetic field side of the magnetic confinement system resulting in an efficient energy transfer between the EM waves and the circulating plasma electrons. For wave-electron energy transfer to occur, the injected EM waves must have an electric field component polarized in the same direction as the electron gyromotion. Additionally, the relative phase between the electron gyromotion and rotating electric field needs to be favourable for acceleration of the plasma electrons. If both of these conditions are met, the plasma electrons are heated resonately.

. These electrons heated in the resonance have a certain probability to collide with gas atoms injected through a different port on the plasma chamber. Such collisions may result in the removal of a single bound electron from any of the electron shells surrounding the nucleus of the atom. This process is referred to as electron impact single ionization. By confining the high energy electrons in the ECRIS, it will ionize atoms and ions in a 'step-by-step' fashion. Each successive ionization will remove a single electron and will eventually lead to

a multiply charged ion. Removal of an electron from one of the inner shells of the atom or inner shell ionization, results in a vacancy in that shell. Such a vacancy can either be filled by a radiative or radiationless transition[2],[3]. If the filling of the vacancy is radiative, a higher lying electron fills the vacancy and a characteristic X-ray is emitted in the process. If the filling of the vacancy is radiationless, a higher lying electron fills the vacancy and a second electron is ejected. This electron is commonly referred to as an Auger electron[4]. An inner shell vacancy can also be filled by Coster-Kronig transitions which are radiationless transitions between subshells having the same principal quantum number[5]. For the purpose of the current discussion, Coster-Kronig transitions will be considered as a special case of the Auger process as the filling of the vacancy is radiationless in both cases.

. Characteristic X-rays, emitted during radiative transitions, can be used as a non-invasive diagnostic tool to study the electron impact ionization process inside the ECRIS plasma. For the results described in this work, we were mostly concerned with transitions from the $2p$ to the $1s$ subshell resulting in $K\alpha$ X-rays, using the Siegbahn notation. Transitions from higher lying shells to the $1s$ subshell are much less probable, but were also included in the measured emission rate. For the rest of this manuscript we will refer to the measured K-emission rate as the $K\alpha$ emission rate with the implicit understanding that it includes $K\beta$ emission as well. The main reason for performing the experiments were to study the influence of the ion source tune parameters on the inner shell ionization rate. In addition, the extracted ion beam currents were also measured in the transfer beamline. This allowed for a comparison between the measured ion beam currents and the inner shell ionization rates, as a function of the source tune parameters. The study therefore allows for a determination of the influence of the changing electron and ion dynamics on the absolute inner shell ionization rate. The $K\alpha$ emission rate from the ECR heated plasma was used to determine the absolute inner shell ionization rate of two different ion sources. The main reason for measuring and comparing the emission rates from two sources were

firstly to cross-check the order-of-magnitude of the absolute emission rate and by implication also the absolute inner shell ionization rate. Secondly the comparison also enabled us to determine if the parametric dependencies are unique to a specific source or the same for both sources. The sources used were the JYFL (University of Jyväskylä, Department of Physics) 14 GHz ECRIS[6] and the 14.5 GHz Grenoble Test Source (GTS)[7],[8] at iThemba LABS (Laboratory for Accelerator Based Sciences). For both ion sources, argon was chosen as working gas, as it is a noble gas and does not get adsorbed on the walls of the plasma chamber. The measured emission rates therefore originate from the plasma and not from the plasma chamber walls. Additionally the efficiency of the X-ray detector, installed in the vacuum, is very close to unity at 2.96 keV ($K\alpha$ of argon)[9]. This made argon a logical choice as working gas from the pool of available noble gases.

. This work could be of particular interest to groups performing numerical simulations on ECRIS plasmas. Modeling of the ECRIS plasma is an exceedingly challenging task, but one that could lead to a better understanding of the physics of the ion source and resulting improvement in its performance. To simulate the ECRIS plasma, ECRIS codes attempt to cover a wide range of phenomena. Some codes use a single particle approach to simulate the heating process inside the plasma[10],[11]. While these codes can evaluate certain plasma parameters with great success it can not account for others like the multiple electron populations present in the ECRIS plasma[11]. Other plasma processes, like collisional processes and ion and electron dynamics, are simulated using codes based on the Particle-In-Cell (PIC) model[11],[12],[13]. Some codes have even been developed to model the space-charge effects during beam extraction and transport[14]. All plasma simulation codes make a number of simplifying assumptions which makes the results of the simulation sensitive to such assumptions. To gauge the success of the simulation, the results of the codes is frequently compared to experimentally determined quantities like the extracted ion beam currents, the sputtering pattern on the plasma electrode and

the beam widths. The current investigation proposes an additional parameter i.e. the $K\alpha$ emission rate against which simulation codes can be benchmarked, a need identified in the literature[15]. As an example, the $K\alpha$ emission rate of argon can be varied by sweeping one of the source tune parameters. This result could easily be simulated by most simulation codes which could output an intermediate parameter for benchmarking purposes.

2. Theoretical background

. As a result of the wave-electron energy transfer and collisional processes occurring inside the ECRIS plasma, the plasma electrons develop into a quasi-continuous energy spectrum which can be described by an electron energy distribution function (EEDF). To determine this distribution function, the ECRIS plasma have in the past been studied using bremsstrahlung diagnostics[16]. From the measured bremsstrahlung spectra, a number of deconvolution schemes have been developed to determine the EEDF[17],[18],[19]. Despite all this effort the real EEDF inside an ECRIS plasma remains not well-known. To complicate matters, the EEDF of the high energy electrons is strongly anisotropic. ECR heating occurs in the plane perpendicular to the magnetic field lines which selectively heats the perpendicular component of the EEDF, not imparting any energy to its parallel component. The perpendicular component therefore has a larger energy than the parallel component. Despite of all the afore-mentioned complications, a multi-component Maxwellian EEDF is commonly assumed for the ECRIS plasma[1]. This is largely because for a Maxwellian EEDF it is convenient to define an electron temperature, kT_e, which is not well-defined for any other distribution function. As a result of the selective heating of the plasma electrons and confinement which strongly depends on the kinetic energy of the plasma electrons, in the absence of collisions, three different electron populations (cold, warm and hot) are thought to exist in an ECRIS plasma[20]. Each of the three electron populations are modelled as a Maxwellian distribution, with a different electron temperature. The warm, 1-10 keV, electron population

of this tri-Maxwellian EEDF is most relevant for inner shell ionization.

. To create a vacancy in the inner shell or K-shell of an ion, confined inside an ECRIS, two processes are of prime importance namely electron-impact excitation and inner shell ionization. Electron-impact excitation of inner shell electrons refers to the process where a target atom (or ion) has an impact with a projectile electron and in the process moves from a lower state ($1s$) to an upper state ($n'l'$), resulting in a vacancy in the K-shell of the atom (or ion). This vacancy can be filled by any of the allowed transitions between the nl-states of the atom (or ion), along with the emission of a characteristic X-ray of transition energy, $E_{1s\rightarrow n'l'}$. The total cross section for electron-impact excitation of inner shell electrons can be estimated using the Van Regemorter formula[21]

$$\sigma_{\mathrm{exe},1s\rightarrow\sum_{n=2}^{\infty} np} = \sum_{n=2}^{\infty} \pi a_0^2 \frac{8\pi f_{1s\rightarrow np}}{\sqrt{3}} \frac{R^2}{E_{1s\rightarrow np}^2} \frac{G_{1s\rightarrow np}(x)}{x} \tag{1}$$

where a_0 is the Bohr radius, $f_{1s\rightarrow np}$ is the absorption oscillator strength, R is the Rydberg energy unit, $G_{1s\rightarrow np}(x)$ is the Gaunt factor, $x = (\varepsilon/E_{1s\rightarrow np})$ and ε is the kinetic energy of the projectile electron relative to the target atom or ion. By comparing the results of the Van Regemorter formula with more accurate computations, the error using this formula was estimated to be as large as an order of magnitude[22]. However, by a proper choice of the Gaunt factor this error can be reduced to 50%, at high energies, for Ar^{17+}[23]. From the discussion above it is clear that excitation to any of the upper states requires a vacancy to exists in those states for the electron to occupy. Thus the number of possible excited states and therefore total excitation cross section depends on the charge state of the ion. Inner shell ionization is very similar to electron-impact excitation with the exception that the bound electron is expelled to the continuum as a result of the impact with the projectile electron. The cross section for inner shell ionization can be determined from the semi-empirical Lotz equation[24]

$$\sigma_{\mathrm{ion}} = a_i q_i \frac{\ln \varepsilon/I_i}{\varepsilon I_i} \{1 - b_i \exp[-c_i(\varepsilon/I_i - 1)]\} \tag{2}$$

where q_i is the number of equivalent electrons in the i-th subshell (for the $1s$ subshell $q = 2$), ε is as defined in equation (1), I_i is the minimum energy required to remove an electron from the i-th subshell (3.21 keV for the K-shell electrons of Ar) and a_i, b_i and c_i are constants which do not strongly depend on the charge state of the ion. It is worth noting that this equation is based on the data available at the time of publishing Ref. [24] (1968) and it is defined for direct electron-impact ionization, not only for the inner shell ionization. For the K-shell, $a_K = 4.0 \times 10^{-14}$ cm^{2}eV^2, $b_K = 0.75$ and $c_K = 0.5$. Lotz estimates the error on the calculated cross sections, using equation (2), to be smaller than 30 - 40 %[24]. The volumetric rate at which K-shell vacancies are produced inside the ECRIS plasma is given by the so-called balance equation[25],[26]:

$$\frac{dN_{K-\text{vacancy}}}{dt} = \sum_{q=0}^{z} n_e n_q^0 \left[\langle \sigma^{q \to q}_{\text{exe},1s \to \sum_{n=2}^{\infty} np} v_e \rangle + \langle \sigma^{q \to q+1}_{\text{ion},1s} v_e \rangle \right] - \frac{n_q^i}{\tau_i} = 0 \quad (3)$$

where n_e is the electron density, n_q is the ion density of ions with charge state q, z is the number of electrons in the considered element and τ_i is the lifetime of the excited state i. The post scripts i and 0 in equation (3) indicate the excited state, generated as a result of a K-shell vacancy, and the ground state, respectively. In writing the balance equation in the above manner, the assumption is made that the system has reached steady-state conditions and the only loss process assumed for the K-shell vacancies is spontaneous transitions. The rate coefficients for inner shell excitation and ionization used in equation (3) are given by the expression[1]:

$$\langle \sigma v_e \rangle = \int f_e(E) \sigma(E) v_e(E) dE \quad (4)$$

where $f_e(E)$ is the prevailing EEDF in the ECRIS plasma, $\sigma(E)$ is the cross section for the process and $v_e(E)$ is the speed of the projectile electrons. From equation (4) the rate coefficient can be determined, as a function of the warm electron temperature, for each of the two processes. This result is shown in figure 1. To calculate the rate coefficients a Maxwellian distribution was used for the warm electrons and as a result of this relativistic effects were not taken into account. At 10 keV the electrons reach approximately 20% the speed of light,

hence this assumption is deemed to be acceptable. The figure clearly shows that ionization plays the dominant role in the generation of K-shell vacancies. This is especially true for ECRIS plasmas in which the densities of high charge states possessing $2p$-vacancies are small in comparison to low charge state ions.

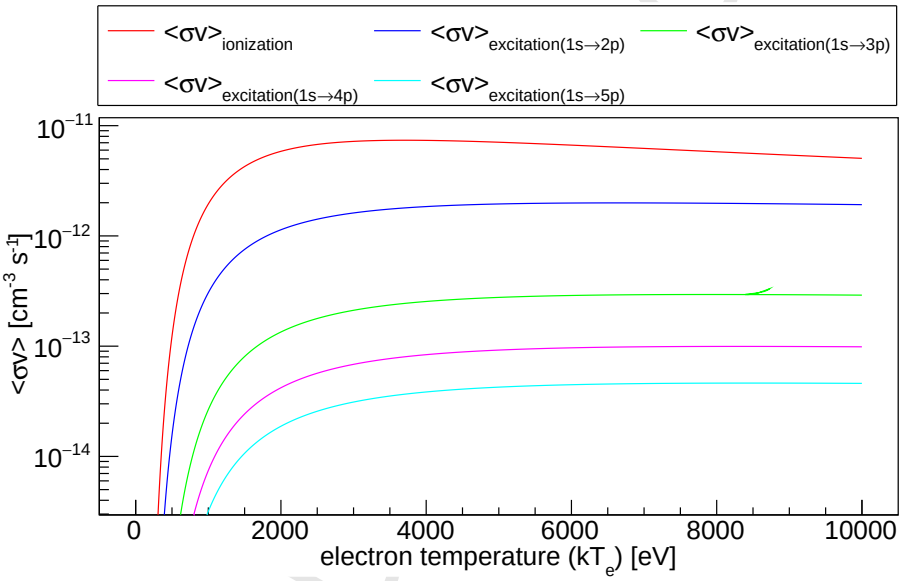

Figure 1: Comparison of the rate coefficients for ionization and excitation to various excited states.

. The observable $K\alpha$ volumetric emission rate (Φ_{R}) is given by the following expression:

$$\Phi_{\mathrm{R}} = K\left[n_e n_n\left(\langle\sigma_{\mathrm{ion}} v_e\rangle + \langle\sigma_{\mathrm{exe}} v_e\rangle\right) + n_e n_i\left(\langle\sigma_{\mathrm{ion}} v_e\rangle + \langle\sigma_{\mathrm{exe}} v_e\rangle\right)\right] \tag{5}$$

where K is a constant that depends on the detector geometry and efficiency and n_i and n_n are the ion and neutral densities, respectively. This expression can be simplified by defining $\langle Q\rangle$ as the average charge state inside the ECRIS plasma and δ as the ionization degree of the plasma. By assuming charge neutrality and expressing n_i and n_n in terms of the ionization degree leads to the expressions:

$$n_i = \frac{n_e}{\langle Q\rangle} \tag{6}$$

$$n_i = \delta n_n \tag{7}$$

Substituting these expressions into equation (5) leads to the simplified form of the observable $K\alpha$ emission rate:

$$\Phi_{\mathrm{R}} = n_e^2 \left(\langle \sigma_{\mathrm{ion}} v_e \rangle + \langle \sigma_{\mathrm{exe}} v_e \rangle \right) \left[\frac{\mathrm{K}}{\langle Q \rangle} \right] \left(1 + \frac{1}{\delta} \right) \tag{8}$$

This expression further simplifies to:

$$\Phi_{\mathrm{R}} = n_e^2 \left(\langle \sigma_{\mathrm{ion}} v_e \rangle \right) \left[\frac{\mathrm{K}}{\langle Q \rangle} \right] \left(1 + \frac{1}{\delta} \right) \tag{9}$$

when the excitation reactions are neglected as justified above. In equations (8) and (9) it is assumed that the total cross section for inner shell ionization and electron-impact excitation is independent of the charge state of the ion. The error in this assumption is mostly due to the excitation cross section which would be larger for very high charge states and smaller for lower charge states. The error in the ionization cross section is largely due to the increased binding energy of the $1s$ electrons, with increasing charge state. In the case of argon, the binding energy of the $1s$ electrons increases by 33% from neutral argon to Ar^{17+}[27]. With the given assumptions the observable $K\alpha$ emission rate depends on electron energy and density (through the rate coefficient), average charge state and ionization degree of the plasma.

. The measured $K\alpha$ emission rate can be correlated with the inner shell ionization rate by taking into account the radiationless de-excitation processes. Once an inner shell vacancy has been produced as a result of the two processes mentioned above, it can be filled by one of three filling mechanisms, as described in section 1. Each of these filling mechanisms has a defined probability of filling the vacancy, the sum of which equates to unity i.e. the vacancy must be filled for the atomic system to reach its lowest energy state.

$$\omega + f + a = 1 \tag{10}$$

ω, f and a in equation (10) are the fluorescence, Auger and Coster-Kronig yields as defined in Ref. [2]. To determine the total inner shell vacancies i.e. total inner

shell ionization and excitation rate, from the measured radiative transitions, a correction needs to be applied for the radiationless transitions. This correction is performed in equation (11) below:

$$n_e n_q^0 \langle \sigma^{q\to q}_{\mathrm{exe},1s\to\sum_{n=2}^{\infty} np} v_e \rangle + n_e n_q^0 \langle \sigma^{q\to q+1}_{\mathrm{ion},1s} v_e \rangle = \frac{\Phi_{\mathrm{R}}}{\omega_K} \tag{11}$$

when only inner shell ionization is considered. Here ω_K is the K-shell fluorescence yield. From the discussion in Ref. [2], the K-shell fluorescence yield can be defined as the ratio of the number of $K\alpha$ characteristic X-rays emitted to the total number of vacancies in the K-shell[2]. This concept was introduced by Barkla in 1918[28]. The K-shell fluorescence yield for argon is 0.118, with an estimated uncertainty of 5-10%[3].

. The prime goal of an ECRIS is the production of multiply charged ions. To achieve this goal, both the number density and temperature of the warm electron population has to be optimized for the desired charge state. One of the major obstacles which opposes multiply charged ion production is charge exchange[1]. This process refers to an interaction between a multiply charged ion and a lower charged ion or atom, in which the multiply charged ion captures a bound electron from the other participant, and in so doing reducing its charge state. Charge exchange affects both the ion densities, and by implication, also the extracted ion beam currents. The influence of charge exchange on the production rate of multiply charged states, can be determined by calculating the mean time between two charge exchange events, τ_{cex}, and comparing it to the mean time between two multiply charged state ionization events, $\tau_{q\to q+1}$. The cross section for charge exchange is highest for interactions with neutral atoms[29],[30], so this process is strongly coupled to the number density of the neutral atoms. By increasing the neutral content of the plasma, the mean time between two charge exchange events decreases resulting in lower high charge state density. To maintain a certain high charge state density with increasing neutral content, the ionization rate should be increased in unison with the neutral content. Due to charge exchange and diffusive losses of high charge states the dependence of inner

shell ionization and high charge state production i.e. extracted beam currents is expected to depend in a different manner on the source tune parameters. This underlines the importance of the $K\alpha$ emission as a diagnostic tool for benchmarking simulations.

3. Experimental setup and data analysis

3.1. Experimental setup

. The volumetric emission rate of the $K\alpha$ X-rays of argon, was studied with the 14 GHz JYFL ECRIS and the 14.5 GHz GTS at iThemba LABS. The JYFL ECRIS has been extensively described in the literature[6] and here only the main features of the source are highlighted. The source is operated at a plasma heating frequency of 14.056 GHz, it has a plasma chamber length of 28 cm and a plasma chamber diameter of 7.8 cm. The biased disc of the JYFL ECRIS is made of stainless steel and it has a diameter of 21 mm. The extraction aperture for the JYFL ECRIS is 8 mm. The magnetic confinement field is provided by two solenoid coils and a permanent magnet hexapole, resulting in magnetic field strengths at injection and extraction of 2.2 T and 0.95 T, respectively. The nominal radial field strength on the magnetic pole is 1.07 T. The base pressure in the source is approximately 1×10^{-7} mbar. In the present configuration the source has one einzel lens to focus the extracted beam.

. The GTS is equipped with two 2.3 kW RF amplifiers, operating at 14.5 and 18 GHz. The radial confinement field is provided by a permanent magnet hexapole with a magnetic field strength of 1.27 T at the plasma chamber wall. The longitudinal magnetic field is produced by three solenoidal coils (injection, extraction and center). The plasma chamber has an active length of 30 cm and a diameter of 7.8 cm. The GTS has a triode extraction system with aperture diameters of 12, 17 and 17 mm for the plasma electrode, intermediate electrode and ground electrode respectively[31]. The source has a tantalum biased disc with a surface area of 12 cm^2, though the disc is not circular. For all the measurements

described in this paper, both sources were operated in continuous wave (CW) mode.

. The main components of the experimental setup, at both JYFL and iThemba LABS, were the detector, the collimator and the digital pulse processor (DP5). In both cases the detector was positioned to measure the axially emitted X-rays from the ECRIS. At JYFL, the detector was positioned to view the plasma through the bending magnet in the transfer beamline, as shown in figure 2a. In the case of the GTS, the detector was positioned in one of the ports of the vacuum chamber of the analyzing magnet, as shown in figure 2b. The distance (D) between the front face of the detector and the extraction electrode of the source is given in table 1. For the measurements described in this work, we used the Amptek X-123SDD X-ray detector[9]. This compact device incorporates the detector, preamplifier, power supplies and DP5 all in one package. Between the detector and the source, the collimator was installed. As an example, the position of the collimator relative to the detector in the experimental arrangement on the GTS is shown in the expanded detailed view B in figure 2b. The collimator was used to eliminate pile-up events and therefore to avoid potential saturation of the measured count rate especially at high microwave power. Additionally the collimator also enabled us to view X-rays emanating from the plasma volume, thus reducing wall bremsstrahlung background. The aperture of the collimator used at JYFL had a diameter of 900 μm and the aperture used at iThemba LABS had a diameter of 500 μm. To protect the detector against charged particles, a permanent magnet filter was included in the experimental setup at JYFL.

. Assuming that the plasma volume visible to the detector can be described by a truncated slightly conical cylinder and the $K\alpha$ emission is uniformly distributed within the plasma chamber volume[1], the volumetric emission rate ($d\Phi_{\mathrm{t}}/dVdt$)

[1]This assumption is discussed in further detail later in this paper.

is given by the following expression[32]:

$$\frac{d\Phi_{\mathrm{t}}}{dVdt} = \frac{4\pi\left(D+\frac{L}{2}\right)^2}{A_{\mathrm{e}}A_{\mathrm{d}}L\left(1+\frac{L}{D}+\frac{1}{3}\frac{L^2}{D^2}\right)}\Phi_{\mathrm{e}} \tag{12}$$

where L is the length of the plasma chamber, D is the distance from the plasma electrode to the entrance of the collimator, $\mathrm{A_d}$ is the area of the collimator aperture in front of the detector and $\mathrm{A_e}$ is the area of plasma electrode aperture. These numbers are given in table 1 for the two different experimental arrangements used at JYFL and iThemba LABS.

Table 1: Geometric dimensions of the different experimental arrangements used at JYFL and iThemba LABS.

	D	L	$\mathrm{A_d}$	$\mathrm{A_e}$
JYFL 14 GHz A-ECR	2627 mm	280 mm	$\pi(0.45\ \mathrm{mm})^2$	$\pi(4\ \mathrm{mm})^2$
14.5 GHz GTS	4032 mm	300 mm	$\pi(0.25\ \mathrm{mm})^2$	$\pi(6\ \mathrm{mm})^2$

. When an X-ray is emitted from the ECR heated plasma, it has a certain likelihood of entering the detector through its 12.5 μm (0.5 mil) beryllium window. Inside the detector, the X-rays create electron-hole pairs in the depletion region of the detector. These charges drift towards the electrodes as a result of the applied bias voltage. This creates a pulse which is proportional to the energy of the incoming x-ray. The anode of the silicon drift detector (SDD), used in this work, is very small and is surrounded by a series of annular drift electrodes. These electrodes guide the electrons through the detector, to be collected at the anode. As a result of the small area of the anode, the total input capacitance of the SDD is very small, which leads to improved energy resolution. The beryllium window of the SDD alters the transmission of the low energy X-rays incident onto the detector. A flux of 1 keV X-rays for example will be attenuated by 76% inside the beryllium window of the SDD[33]. Similarly the finite width of the active region of the detector, limits high energy X-rays from

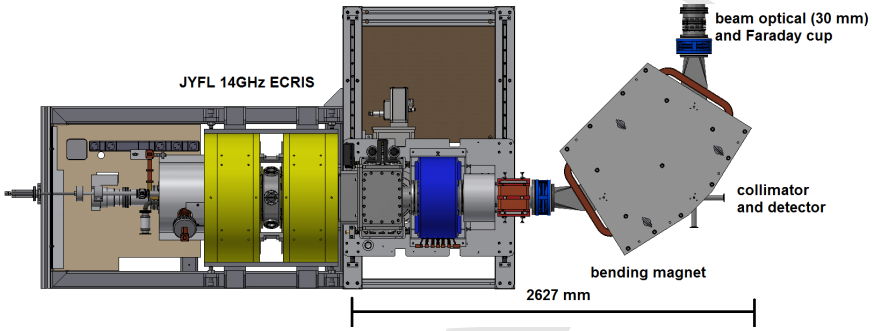

(a) Schematic of the JYFL ECRIS and connecting transfer beamline elements. The two ports of the bending magnet are also shown. The X-ray detector (not shown) was attached to the one port enabling it to view the ECR plasma axially through the bending magnet.

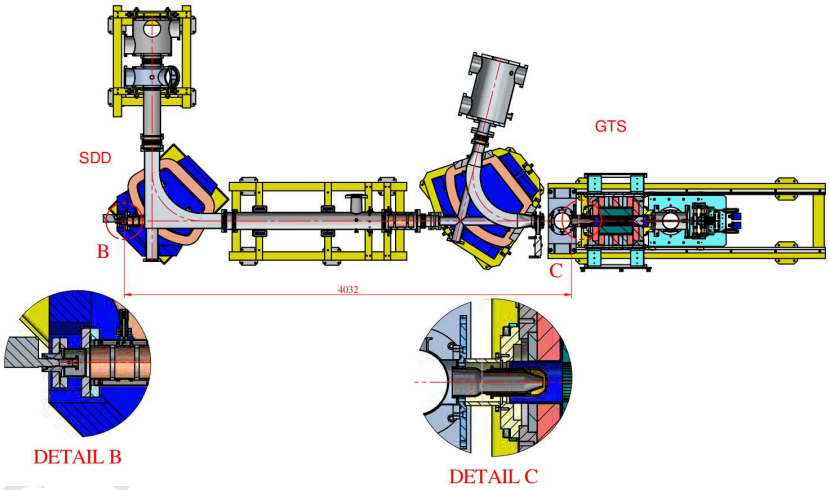

(b) Layout of the experimental arrangement at iThemba LABS showing the GTS and the position of the SDD.

Figure 2: Schematic view of the experimental arrangements used at JYFL and iThemba LABS.

being detected. This effect refers to the efficiency of the X-ray detector. At the 2.96 keV energy of the $K\alpha$ of argon, approximately 86% of the $K\alpha$ X-rays is detected in the 450 μm thickness of the active region of the SDD[9]. Both these transmission and efficiency effects had to be taken into account in translating the measured $K\alpha$ emission rate into a volumetric emission rate and inner shell ionization rate.

3.2. Data Processing

. The DP5 digitizes the preamplifier output from the detector. Inside the DP5, pulse shaping is done with a digital shaping amplifier. The advantage of digital shaping amplifiers over analog shaping amplifiers are well documented[9]. In the case of our measurements, a digital trapezoidal shaper was used. With such a trapezoidal shaper the so-called 'peaking time' and 'flat top time' can be specified independently. In this way one can minimize the pile-up and maximize the count rate. The peaking time and flat top time was set to 4.8 μs and 100 ns, respectively for all the measurements performed in this work. Since the peaking time influences the energy resolution of the detector, this parameter had to be determined as a function of peaking time. At the peaking time used for our measurements, the energy resolution was determined to be 160 eV at the $K\alpha$ of Mn (5.9 keV). The data was acquired with custom software supplied by Amptek. The digitized output of the slow channel is stored in the FIFO (First-In First-Out) memory, along with its time-stamped information. This method of organizing data entails that the data first read into the memory will be lost first if the memory capacity is exceeded. This information is readout to a host computer via the USB port every 10 ms. As long as the readout rate exceeds the rate of writing data to the FIFO, the FIFO never overflows and no data is lost. With the acquisition software, piled-up events were tagged to be dealt with later during the analysis. The DP5 allows for piled-up events to be identified by determining the time difference between two incoming X-rays on the fast channel. If this time difference is less than the sum of the peaking time and flat top time, the event is tagged as pile-up. With the implementation of

the collimator, pile-up was reduced to less than 0.001%.

. To determine the volumetric emission rate of the $K\alpha$ of argon, the measured spectrum was firstly corrected for the X-ray losses in the beryllium window, as well as for the efficiency of the detector. Following this, the background spectrum generated by the combined effects of the plasma and wall bremsstrahlung was subtracted from the corrected spectrum. In the case of the work presented in this paper, the background was determined using a ROOT function[34]. This function is based on the so-called Sensitive Peak Clipping Algorithm (SNIP)[35],[36] and allows for continuous background to be extracted from a measured spectrum. A Gaussian peak was then fitted to the $K\alpha$ of argon. The number of counts between the 10% threshold on either side of the peak of the Gaussian was then determined. By integrating between the two 10% thresholds, the number of counts in the integration corresponds to roughly 2σ of a Gaussian distribution. The number of counts is then averaged over the measurement time to yield Φ_e. Figure 3 and 4 show typical spectra recorded from the two ion sources.

. Comparing figure 3 with figure 4, reveals the difference between the two sources from an X-ray spectral point of view. For both sources, the line-of-sight of the X-ray detector ends at the biased disc, which enables the detector to measure characteristic lines from the material of the biased disc. As discussed in section 3.1, the material of the biased disc in the GTS and the JYFL ECRIS differ. Table 2 shows the most prominent lines observed in the X-ray spectra of the two sources, along with their intensity normalized with respect to the counts in the $K\alpha$ of argon. The measured GTS X-ray spectrum shown in figure 4, has various characteristic lines emanating from the tantalum biased disc. These lines are not observed in the case of the JYFL ECRIS, instead strong lines are observed from the composites of stainless steel coming from the stainless steel biased disc. The X-ray spectra taken from the JYFL ECRIS also reveals strong aluminium and chromium lines. The aluminium lines most probably emanate from backstreaming electrons which interact with the aluminium

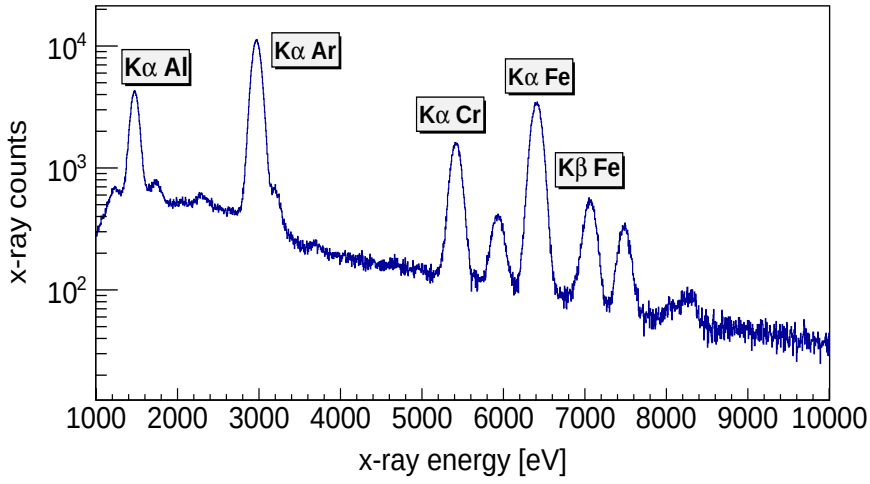

Figure 3: A typical X-ray spectrum measured from the ECRIS plasma of the JYFL ECRIS with a few prominent lines being identified. The bremsstrahlung background has not been subtracted in this spectrum.

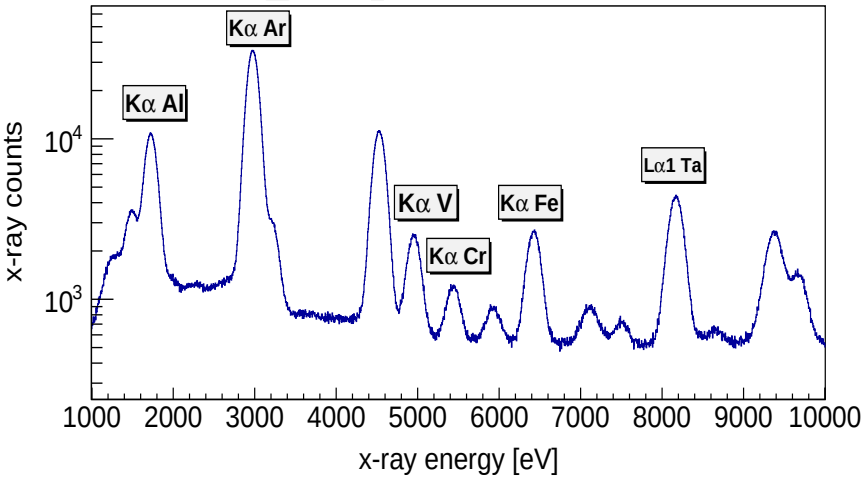

Figure 4: A typical X-ray spectrum measured from the ECRIS plasma of the GTS with a few prominent lines being identified. The bremsstrahlung background has not been subtracted in this spectrum.

extraction system of the source. The extraction electrodes of the GTS are made of stainless steel which most likely accounts for the lines of the stainless steel composites observed in the case of the GTS. The chromium lines observed with the JYFL ECRIS most probably originates from residues accumulated on the plasma chamber surface from previous ion source operation, as well as from the biased disc. The fact that both plasma chambers are made of aluminium and weak aluminium lines are observed with the GTS spectra leads us to believe the contribution from the plasma chamber to the aluminium lines is insignificant. The $K\alpha$ of argon is the dominant peak in both spectra which implies that the contribution of the confined electrons is more prominent in comparison to lost electrons creating characteristic X-rays and bremsstrahlung on the surfaces.

Table 2: Most prominent characteristic lines observed in each of the X-ray spectra measured on the two ion sources. The measured number of counts in each of the lines was normalized with respect to the $K\alpha$ counts of argon. The symbol (-) implies that the lines could not be detected as their intensity is below the threshold of the detection system.

Characteristic line energy (Siegbahn notation)	iThemba LABS GTS (%)	JYFL A-ECR (%)
1.5 keV (Kα Al)	5.8	19.8
1.7 keV (Mα1 Ta)	24.8	-
3.0 keV (Kα Ar)	100	100
4.5 keV (Kα Ti)	15.4	-
4.9 keV (Kα V)	4.3	-
5.4 keV (Kα Cr)	3.5	25.9
5.9 keV (Kα Mn)	2.5	8.5
6.4 keV (Kα Fe)	4.7	58.9
7.1 keV (Kβ1 Fe)	2.8	10.9
7.5 keV (Kα Ni)	-	6.6
8.1 keV (Kα Cu)	6.4	-
9.4 keV (Lβ Ta)	8.7	-

3.3. Analysis of the sources of error

. During the process of acquiring the data, a number of sources of error were identified. These will be briefly discussed in this section. The measurements were performed over many hours to accumulate sufficient statistics. Over such extended measurement periods, the source tune could change. These changes could alter the measured volumetric emission rate. To assess the influence of this uncertainty on the results, the volumetric emission rate was measured at three different times during the measurement campaign, at the same source setting. This comparison gave an indication of systematic error as well as the changing volumetric emission rate with time. This led us to conclude that the sum of these two effects results in an uncertainty of 12.5% in the measured emission rate. Another source of error is the difference between the measurement time and the acquisition time. The detector has a charge sensitive preamplifier, which produces a voltage proportional to the time integral of the current[9]. The integrator in the preamplifier saturates with time and needs to be reset. During reset, data acquisition is temporarily stopped. In determining the count rate, the measurement time was not corrected for these reset intervals. Since the reset interval was set to 102 μs and the measurement time extended for up to thirty minutes, the error in determining the count rate is deemed small.

. An error was also incurred as a result of the alignment of the detector relative to the magnetic axis of the source. In the case of the measurements performed with the GTS, the detector was placed in a port on the vacuum chamber of the bending magnet. As the bending magnet had to be aligned with the magnetic axis of the source, the alignment in this case was deemed small. In the case of the measurements performed on the 14 GHz ECRIS at JYFL, the detector was also mounted in a port in the vacuum chamber of the bending magnet. The vacuum chamber of the magnet is however not firmly attached to anything which makes alignment of the detector rather tricky. The initial alignment was checked with a theodolite relative to a reference point on the transfer beamline. With the detector installed, the alignment was fine tuned by making minor

adjustments and looking at the total count rate measured by the detector. At roughly maximum count rate, the detector position was fixed. The error on the alignment results in an error on the effective radius of the collimator as seen by the X-rays. Due to the uncertainty related to the alignment, the effective diameter of the collimator is estimated to 600-800 μm.

. To determine the volumetric emission rate the initial assumption is made that the $K\alpha$ emission originates from a point source in the centre of the plasma volume. Given the large distance of the detector from the plasma volume, the emission closely resembles that of a point source. The error in this assumption is therefore deemed to be very small as described thoroughly in the literature[32]. To translate the point source like emission into a volumetric emission rate using equation (12), a further assumption is made that the emission from the volume visible to the detector is spatially uniform as well as isotropic. In reality, it is well-known that the electron, ion and neutral distributions are not uniform inside the plasma volume. The heated electron populations are strongly collisionless and therefore magnetically confined. The magnetic confinement field therefore dictates the electron distribution inside the ECRIS. Given the very short lifetime of a K-shell vacancy (typically nanoseconds), $K\alpha$ emission occurs almost instantaneously after the generation of a K-shell vacancy. This implies that the ions and neutrals do not move significant distances between a K-shell vacancy generation and $K\alpha$ emission. The neutrals and ions therefore form a background of targets, in the vicinity of the heated electrons, which collides with the heated electrons. It can therefore be argued that the $K\alpha$ emission distributions are dictated by the magnetic confinement field. From the results obtained from numerical simulations it is believed that the plasma density is higher inside the ECR zone[11]. The assumption of uniform $K\alpha$ emission therefore corresponds to the lower limit of the volumetric emission rate, in absolute terms. Since the plasma does not fill the entire volume described by equation (12), the true volumetric rate is higher than the result obtained. The upper limit for the volumetric emission rate can be calculated by assuming there is

a dense plasma inside the ECR zone and using the volume of the ECR zone to calculate the volumetric emission rate in equation (12). In the case of the JYFL 14 GHz ECRIS, for example, the axial length of the ECR zone is 80 - 90 mm at typical magnetic field settings. This translates to the upper limit of the volumetric emission corresponding to concentrated emission profile to be 3.1 - 3.5 times the lower limit corresponding to a uniformly distributed emission. The real volumetric emission rate is most likely between these two limits.

4. Experimental results

4.1. Influence of the microwave power and neutral gas pressure on the absolute inner shell ionization rate

. The influence of the microwave power and neutral gas pressure on the absolute inner shell ionization rate was studied with the JYFL 14 GHz ECRIS. With this investigation, the source was tuned for a high charge state (Ar^{13+}) and for the first part of the investigation the incident microwave power was varied between 100 W and 600 W, at a fixed neutral gas pressure. All other source parameters were kept at constant settings shown in table 3.

Table 3: Ion source settings for the microwave power sweep.

calibrated pressure at injection (0 W)	4.3×10^{-7} mbar
B_{inj} (magnetic field strength at injection)	2.02 T
B_{min} (B minimum)	0.35 T
B_{ext} (magnetic field strength at extraction)	0.95 T A
biased disc voltage	-170 V
microwave power	100 - 600 W

. It has been shown previously that the microwave power absorbed by the plasma changes as the incident microwave power changes[37]. To estimate the absorbed microwave power, the microwave power losses in the waveguide were

estimated to be 20% of the incident microwave power. These power losses were subtracted from the incident microwave power to yield the power absorbed by the plasma. Due to an impedance mismatch between the klystron and the plasma load and transmission system, a fraction of the forward power gets reflected in the transmission system. In the case of measurements performed at JYFL, the reflected power was estimated to be less than 2% of the forward power. The absorbed power, as defined here, is however only an estimation of the maximum possible power that can be absorbed by the plasma. Besides power losses and reflection in the waveguide, various other possible power dissipation channels exist, for example losses in the plasma chamber, high voltage break and vacuum window. The variation of the absolute inner shell ionization rate with increasing absorbed microwave power, at different neutral gas pressures, is shown in figure 5. By propagating the uncertainties in the alignment, the systematic error and K-shell fluorescence yield, the uncertainty in the absolute inner shell ionization rate, as presented in figure 5, was determined to be $\pm 32\%$. Additionally the presented absolute inner shell ionization rates were also corrected for vacancies generated as a result of inner shell excitation, to take this process into consideration. Lastly it should be mentioned that the absolute inner shell ionization rates shown in figure 5 is the estimated lower limit due to the assumption of uniformly distributed and isotropic emission.

. From the discussion in section 2 it is known that the observable $K\alpha$ emission rate, and therefore also the absolute inner shell ionization rate, depends on the average charge state and ionization degree of the plasma, as well as on the electron energy and density. It is commonly assumed that the charge state distribution (CSD) of the plasma core differs from the extracted CSD[15], but the extracted CSD can be used to gain insight into the changing plasma core CSD during a parametric sweep. During a typical microwave power sweep, the variation of the average extracted charge state observed was from 7.98 to 10.45. These average extracted charge states were however calculated for argon only and it should be emphasized that any impurities present within the plasma will

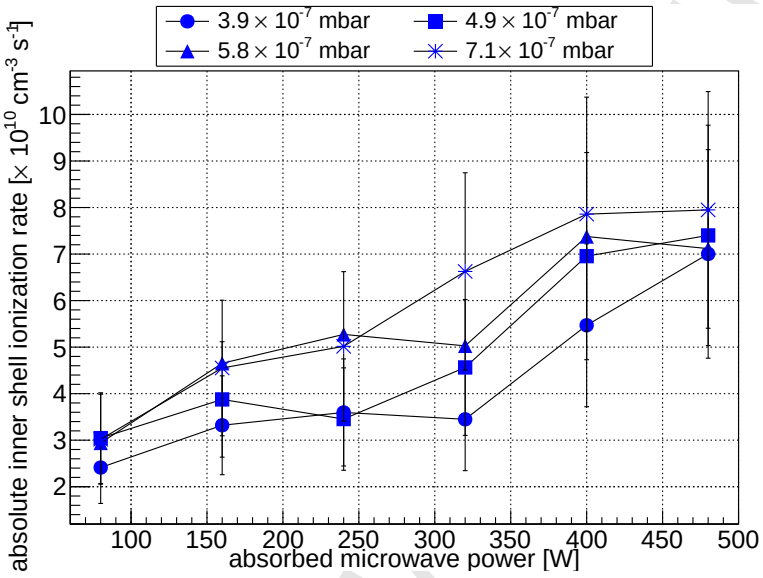

Figure 5: Variation of the (minimum) absolute inner shell ionization rate as a function of absorbed microwave power, at different neutral gas pressures.

decrease the average charge state. Also, to determine the average extracted charge state, the low charge states had to be estimated as these can not be measured due to limitations on the analyzing magnet. To estimate the low charge state, a particle spectrum was formed and an envelope curve fitted over the particle currents. The low charge state particle currents determined from the envelope curve were most likely underestimated and additionally all charge states are subjected to losses in the transmission line. All these factors enhance the difference between the plasma core CSD and the extracted CSD. In comparison to the variance of the average extracted charge state, the typical variation in the absolute inner shell ionization rate during the same parameter sweep was determined to be between $8.80 \times 10^9 \mathrm{cm}^{-3}\mathrm{s}^{-1}$ and $3.00 \times 10^{10} \mathrm{cm}^{-3}\mathrm{s}^{-1}$. The relative variation of the absolute inner shell ionization rate (during the parameter sweep) is at least three times more than the estimated variation in the average charge state of the plasma core. This implies that the average charge state of the plasma core probably plays a lesser role in comparison to the other plasma

parameters which affect the inner shell ionization rate. Thus, the increase of inner shell ionization rate with microwave power is most likely due to increasing plasma energy content, $n_e kT_e$, as deduced from experiments on ECRIS plasma diamagnetism[38].

. The influence of the ionization degree on the absolute inner shell ionization rate can be established by determining the efficiency of producing inner shell ionization per unit absorbed microwave power. Figure 6 shows that the rate of producing inner shell ionization, per unit of absorbed microwave power, is highest at the lowest absorbed microwave power. This implies that inner shell ionization is most effectively produced at low degree of ionization of the plasma. The figure also shows that the inner shell ionization rate, per unit absorbed power, saturates as the absorbed power is increased. Since the behaviour of the ionization rate and production efficiency (reported in Ref. [39]) with increasing microwave power is logarithmic, the curves in Fig. 6 illustrate the inverse behaviour of the $K\alpha$ emission rate and the ionization rate.

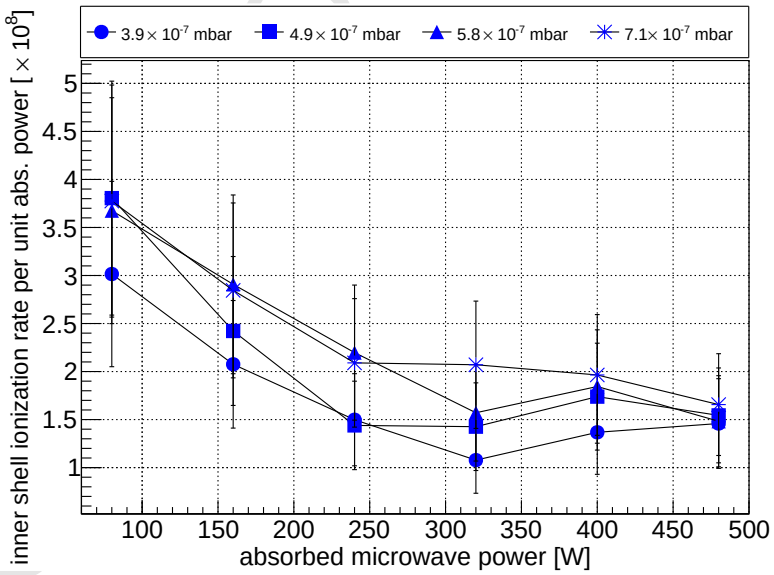

Figure 6: Variation of the (minimum) absolute inner shell ionization rate per unit absorbed microwave power, at different neutral gas pressures.

. The observations from figure 6 can be explained by assuming that the ions and neutrals behave as an ideal gas. Neutral atoms are typically considered to be cold ($kT_{\text{neutral}} \approx 25$ meV at room temperature), while the ion temperature (kT_{ion}) is typically between 1-5 eV[26]. This implies that the total density of argon (atoms and ions) decreases with increasing ionization degree, which (along with the average charge state) could presumably explain the behaviour observed in figure 6. At low absorbed microwave power, the ionization degree and energy content of the plasma is still very low. The neutrals therefore make up a sizeable fraction of the plasma constituents. This larger neutral content presumably leads to the increased inner shell ionization rate, averaged over the absorbed microwave power, as observed in the experimental results. As the degree of ionization of the plasma increases, with increasing absorbed microwave power, the neutral content becomes less. This leads to the decreased inner shell ionization rate, averaged over the absorbed microwave power.

. Based on the discussion above, it can be concluded that the absolute inner shell ionization rate is affected by the ionization degree of the plasma. The influence of the electron energy and density i.e. the plasma energy content on the absolute inner shell ionization rate becomes more pronounced as the absorbed microwave power increases as seen in Fig. 5. The saturation of the inner shell ionization rate per unit of absorbed microwave power is consistent with the saturation of the plasma energy content as a function of microwave power, reported in Ref. [38]. The relative large error bars of the absolute inner shell ionization rate do not affect these tendencies since the error is considered to be mostly systematic (due to the given assumptions) as described in section 3.3.

. To relate the absolute inner shell ionization rate to the extracted CSD, the faraday cup current of a high (Ar^{13+}) and low (Ar^{6+}) charge state were compared to the absolute inner shell ionization rate. Figure 7 presents the faraday cup currents of the two different charge states during the microwave power sweep, at different neutral gas pressures. By comparing figure 7a with figure 5,

it is observed that the absolute inner shell ionization rate and Ar^{13+} production shows some resemblance i.e. both quantities increase with increasing absorbed microwave power. The reason for the observed trend is most likely due to the increasing average charge state of the plasma, as well as the increasing plasma energy content. From the comparison of figure 7b and figure 5 it can also be remarked that the absolute inner shell ionization rate and the Ar^{6+} production appear to have opposing trends i.e. the absolute inner shell ionization rate increases while the Ar^{6+} production decreases. The Ar^{6+} current presumably decrease due to the CSD shifting towards higher charge states which is caused by the increasing plasma energy content.

. For the second part of this investigation the variation of the absolute inner shell ionization rate, with neutral gas pressure, was probed. With this investigation the same source settings as given in table 3 was used, with the incident microwave power fixed and the neutral gas pressure varied between 2.5×10^{-7} mbar to 1.1×10^{-6} mbar. The values of the neutral gas pressures were obtained without igniting the plasma. The results of this set of measurements is shown in figure 8. Previous studies investigating the X-ray power emitted by the confined electrons of an ECRIS proposed a saturation of the X-ray power with increasing neutral gas pressure[38]. These studies however focused on the X-ray emission from the plasma bremsstrahlung. With the current investigation it was found that the behaviour of the $K\alpha$ emission rate with increasing neutral gas pressure, and by implication also the absolute inner shell ionization rate with increasing gas pressure, behaves very similar to the results obtained in the cited reference. The inner shell ionization rate was found to initially increase rapidly with increasing neutral gas pressure. The rapid increase in absolute inner shell ionization rate is most likely due to the increase in the target densities (atoms and ions), as well as the electron density. The rapid increase in electron density with increasing pressure is also simulated by some ECRIS codes[40]. The rate of increase becomes larger as the microwave power is increased. This most likely points to the increased contribution to inner shell ionization due to

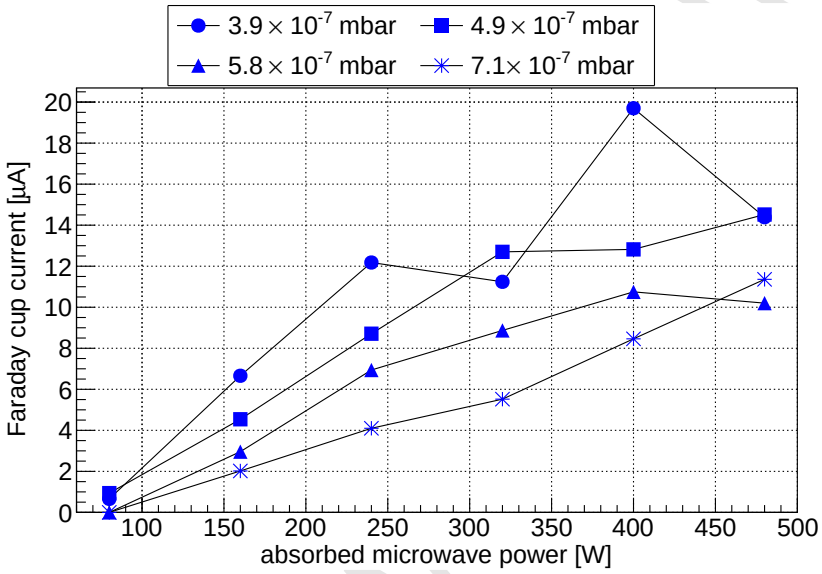

(a) Faraday cup current of Ar^{13+} as a function of the absorbed microwave power, at different neutral gas pressures.

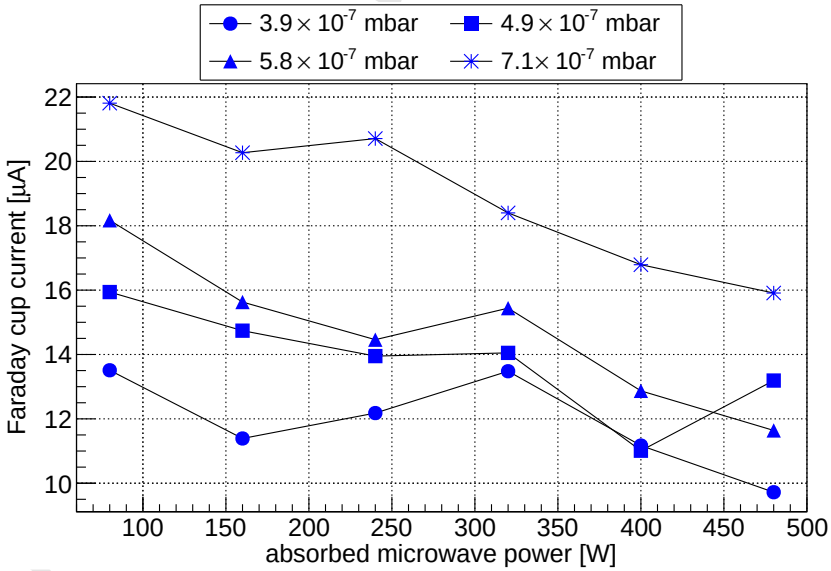

(b) Faraday cup current of Ar^{6+} as a function of the absorbed microwave power, at different neutral gas pressures.

Figure 7: Faraday cup current of Ar^{13+} and Ar^{6+} as a function of the absorbed microwave power, at different neutral gas pressures.

the increasing plasma energy content, with increasing microwave power. With further increase in pressure, the inner shell ionization rate reaches a saturation point. At this point the energy content of the plasma is considered insufficient to sustain any further growth in the ionization degree of the plasma. This assertion is supported by the saturation in the production rate of high charge states observed in the measured extracted charge state distribution as shown in figure 9. With even further increase in pressure, the charge exchange process becomes more dominant and results in a decrease in the extracted currents of high charge states. This is evident from the substantial decrease in Ar^{11+}, with increasing pressure, observed from the extracted CSD shown in figure 9.

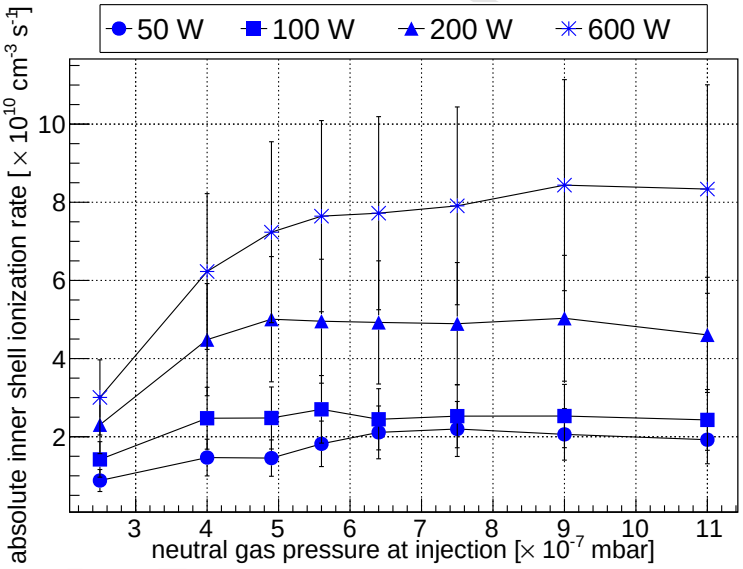

Figure 8: Variation of the (minimum) absolute inner shell ionization rate as a function of gas pressure, at different incident microwave powers.

. To complete the investigation into the influence of the pressure sweep on the absolute inner shell ionization rate, the low and high charge state production as a function of the pressure sweep was also considered. From the discussion above it is known that the absolute inner shell ionization rate initially increases very

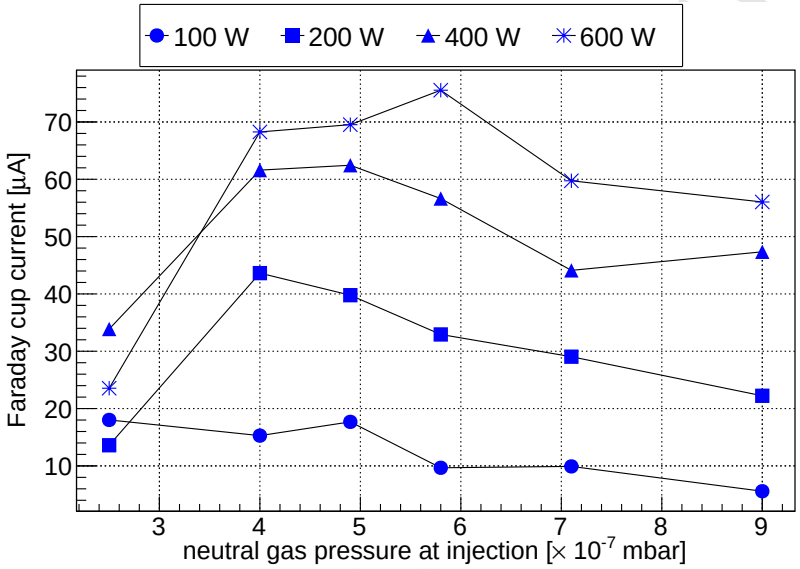

Figure 9: Faraday cup current of Ar^{11+} as a function of the neutral gas pressures, at different incident microwave powers.

sharply with pressure increase, at a fixed microwave power. This increase becomes more pronounced at higher microwave power. From the extracted charge state distribution, the general trend observed was for high charge state production to decrease as the pressure is increased, at a fixed incident microwave power as shown in figure 10a. This observation can be explained by referring to the discussion in section 2. From the discussion there it is known that the charge exchange process dominates if the confinement time needed for high charge state production becomes greater than the time between two charge exchange events. By increasing the neutral pressure, this situation is realized resulting in the decreasing high charge state production. It was also observed that the optimum high charge state production occurs at low pressures and increases to higher pressure, as the microwave power is increased. From this observation it is concluded that the increasing inner shell ionization rate observed at low pressure results in increased high charge state production. As the pressure is further increased, at a fixed microwave power, the inner shell ionization rate increases

but the high charge state production initially saturates and then decreases presumably due to increased rate of charge exchange reactions. As the microwave power is increased, the optimum high charge state production is reached at higher pressures. As an example, at 100 W of incident microwave power, the optimum Ar^{13+} production occurs at 2.5×10^{-7} mbar. At 600 W of incident microwave power, the optimum Ar^{13+} production occurs at 4.9×10^{-7} mbar. From the measured extracted CSD, the optimum pressure for Ar^{11+} production also increases monotonically with increasing absorbed microwave power. These observations suggest that the energy content of the plasma, for optimum high charge state production, is strongly influenced by the change in pressure.

4.2. Influence of the magnetic field configuration and biased disc voltage on the absolute inner shell ionization rate

. The absolute inner shell ionization rate was also studied as a function of the magnetic field configuration and biased disc voltage. This investigation was again performed with the JYFL 14 GHz ECRIS, with the source tuned for optimum Ar^{13+} production. The corresponding source settings are given in table 3. For the first part of the investigation the incident microwave power was fixed at 400 W, with only the solenoid coil currents being changed. In all measurements reported in this work, the injection and extraction coil currents were kept equal. As the source has a permanent magnet hexapole, the magnetic field contribution from this element remained constant during the investigation. When considering the influence of the magnetic field configuration, most literature only report on changes as a function of magnetic field parameters like the mirror ratio, $B_{\mathrm{min}}/B_{\mathrm{ECR}}$-ratio and the on-axis magnetic field gradients at injection and extraction. While these parameters certainly play an instrumental role during electron heating, it in a sense trivializes the heating process by considering only the magnetic field gradient at certain regions in the ECR zone, for example. It can be argued that the magnetic field gradient at these points do not alone influence the heating, but the heating is influenced by the gradient at all points over the ECR surface. The approach therefore employed in this

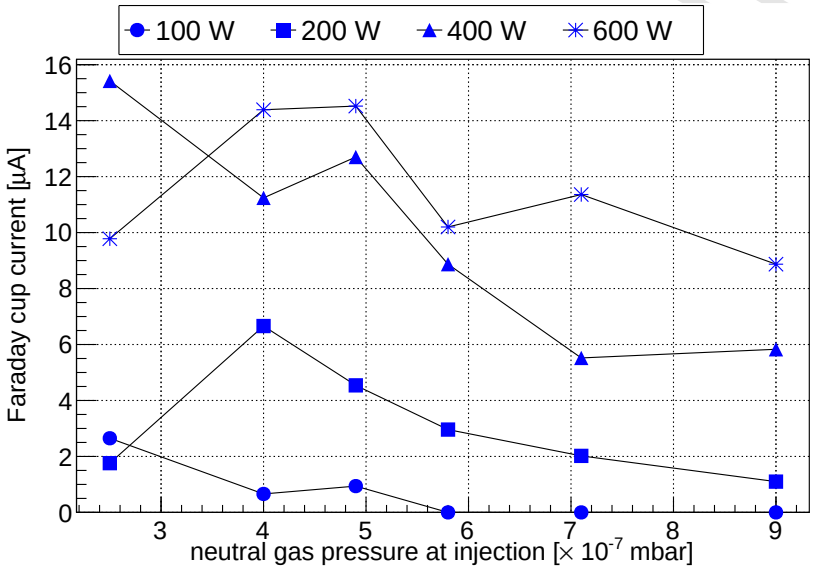

(a) Faraday cup current of Ar^{13+} as a function of neutral gas pressure, at different incident microwave powers.

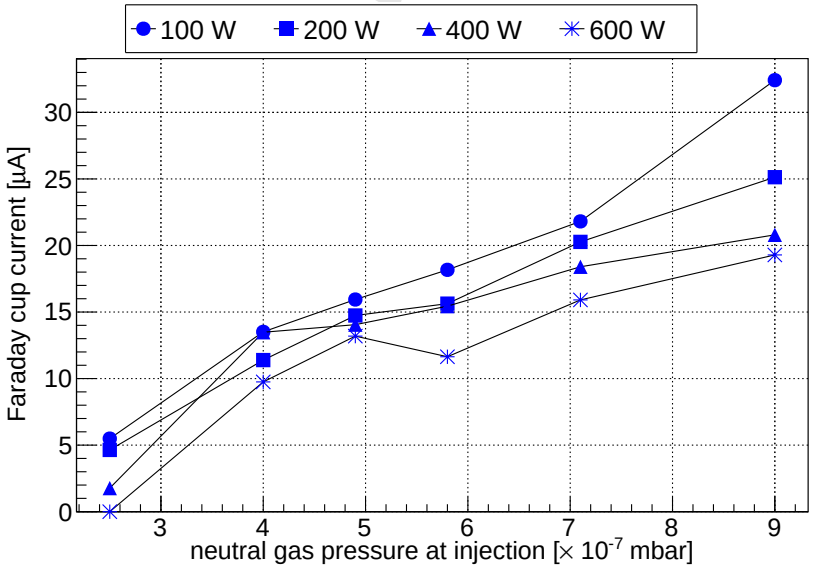

(b) Faraday cup current of Ar^{6+} as a function of neutral gas pressure, at different incident microwave powers.

Figure 10: Faraday cup current of Ar^{13+} and Ar^{6+} as a function of neutral gas pressure, at different incident microwave powers.

work is to consider the average magnetic field gradient in the direction parallel to the field lines across the entire ECR surface, as was done in ref [41].

. The variation of the absolute inner shell ionization rate as a function of average parallel magnetic field gradient and $B_{\mathrm{min}}/B_{\mathrm{ECR}}$-ratio is presented in figure 11a. The results of this investigation seems to indicate that the inner shell ionization rate is decoupled from changes to the magnetic field configuration. In changing the solenoid coil currents from 570 A to 490 A, the average parallel magnetic field gradient over the ECR surface changed from 4.03 T/m to 7.53 T/m, while the $B_{\mathrm{min}}/B_{\mathrm{ECR}}$-ratio changed from 0.825 to 0.683. The maximum change in inner shell ionization rate observed over the magnetic field sweep amounted to 29%, which is within the error bars of the measurement. This is in contrast with the microwave power and pressure sweeps, where changes in absolute inner shell ionization rate in excess of 400% were observed. This seems to indicate that the magnetic field changes have very little impact on the warm electron population of the ECRIS. Previous investigations determining the so-called spectral temperature also noted minimal changes of this parameter as a function of $B_{\mathrm{min}}/B_{\mathrm{ECR}}$[38]. The spectral temperature is equivalent to a mean electron temperature defined over a certain energy range. In the cited investigation, the spectral temperature was determined over a range (4-20 keV) very close to the binding energy of the $1s^2$ electrons of argon. From the spectral temperature results in Ref. [38], it appears as if the magnetic field sweep has a larger impact on the hot electron population.

. To gauge the influence of the parameter sweep on high charge state production, the extracted Ar^{13+} beam current was used, as shown in figure 11b. The largest extracted Ar^{13+} intensity is achieved with the solenoid coil currents set to 550 A. Simultaneous optical emission measurements through the radial diagnostics port viewing the core plasma and probing the intensity of the $2s^2 2p^2\ P^{\circ}_{3/2} \longrightarrow 2s^2 2p^2\ P^{\circ}_{1/2}$ transition of Ar^{13+} confirmed that the Ar^{13+} density indeed is maximized at this coil current setting where the peak of the inner shell ionization is also achieved. At 550 A, the average parallel magnetic field gradient

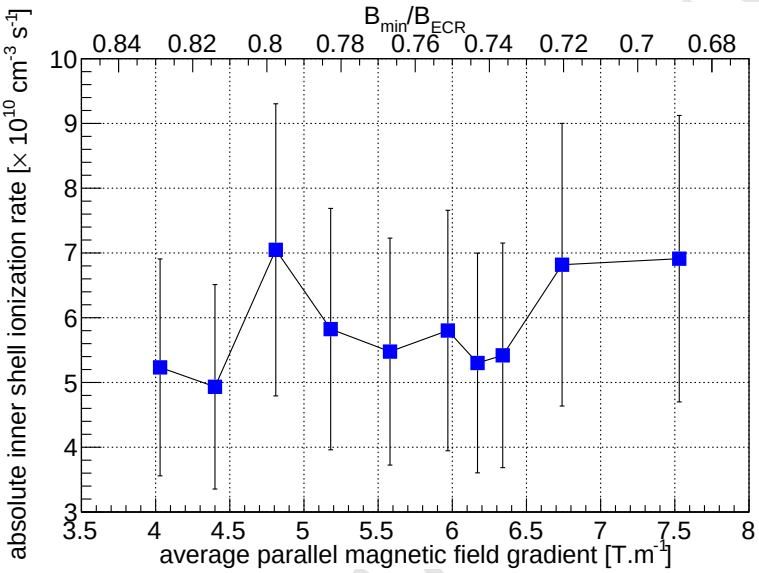

(a) Variation of the (minimum) absolute inner shell ionization rate as a function of average parallel magnetic field gradient and $B_{\mathrm{min}}/B_{\mathrm{ECR}}$-ratio.

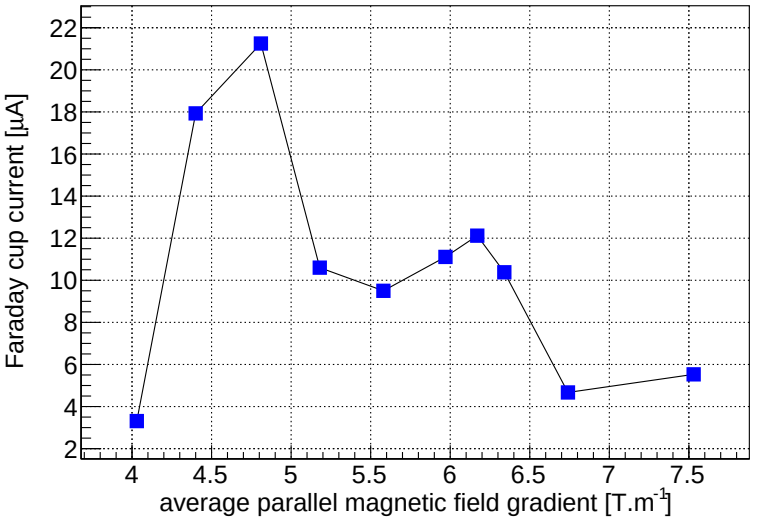

(b) Faraday cup current of Ar^{13+} as a function of average parallel magnetic field gradient.

Figure 11: Variation of the (minimum) absolute inner shell ionization rate as a function of average parallel magnetic field gradient and $B_{\mathrm{min}}/B_{\mathrm{ECR}}$-ratio and Faraday cup current of Ar^{13+} as a function of average parallel magnetic field gradient.

over the ECR surface was determined to be 4.81 T/m. As a result of this strong axial magnetic field, the average gradient is low which results in efficient heating of the plasma electrons. This results in an enhanced hot electron population trapping more ions through its ambipolar potential. These ions are confined for long times which ultimately leads to the higher Ar^{13+} beam intensity as shown in the figure above. At the same time the total ion current extracted from the source is decreased as the improved confinement affects the integrated flux of ions towards extraction i.e. the charge state distribution and dynamic equilibrium of charge particle losses are both affected by the strength of the magnetic field. As the coil current is further increased, the plasma becomes prone to plasma instabilities[41],[42]. These instabilities manifest as beam instabilities, clearly observed in the extracted beam current at solenoid coil currents $\geq$ 560 A. The plasma instabilities were also observed with a microwave detector installed in the waveguide of the source. The plasma instabilities reduce the ion confinement time, as electrons are continuously expelled from the magnetic trap which decreases the ion confinement time and extracted current of highly charged ions[41].

. The influence of the biased disc voltage on the absolute inner shell ionization rate was also studied with the JYFL 14 GHz ECRIS. From the literature it is proposed that by increasing the negative voltage applied to the biased disc, the confinement of low energy electrons is improved[43],[44]. Previous investigations at JYFL have not observed any change of the bremsstrahlung emission as a result of the changes to the biased disc voltage. In the current investigation, the variation of the $K\alpha$ emission rate as a function of biased disc voltage was probed. As with the other parameter sweeps, the source was again tuned for optimum Ar^{13+} production. The source settings for this investigation are given in table 3, with the incident microwave power fixed at 400 W, and only the biased disc voltage varied. Similar to the magnetic field sweep, the variation of the absolute inner shell ionization rate with biased disc voltage was minimal as shown in figure 12. Over the entire range of the voltage sweep, the maximum

variation in absolute inner shell ionization rate measured was 31% which was again within the experimental uncertainty. This meagre variation leads to the conclusion that the biased disc voltage sweep has no direct impact on the warm electron population. From measurements performed on the JYFL 6.4 GHz ECRIS, it was concluded that the plasma potential decreases with increasing negative biased disc voltage[43]. This observation leads to the conclusion that the biased disc voltage repels electrons back into the plasma and enhances ion losses axially at the injection side of the source. Given the relatively small voltage applied to the biased disc (≤ -300 V), it is suggested that the biased disc only acts on cold electrons and, thus, the effect on the inner shell ionization caused by the warm electrons is insignificant.

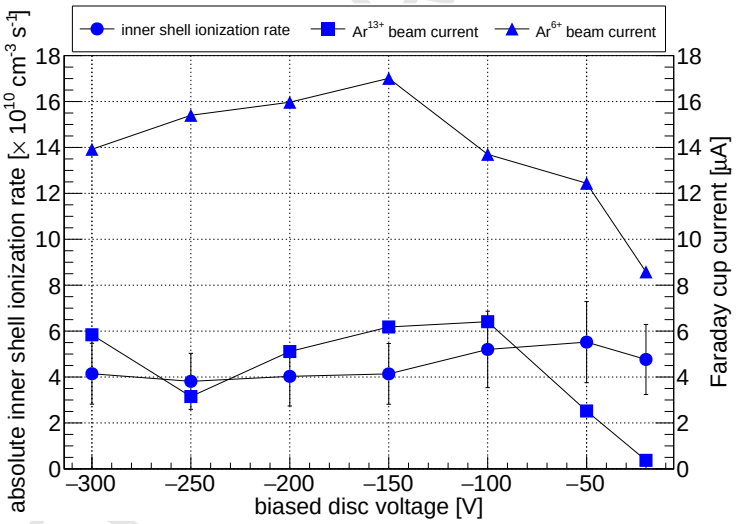

Figure 12: Variation of the (minimum) absolute inner shell ionization rate as a function of biased disc voltage as well as the Faraday cup current of Ar^{13+} and Ar^{6+}.

. To relate these observations to high charge state production, the inner shell ionization rate as a function of the voltage sweep was compared to the production rate of Ar^{13+} as shown in figure 12. Between -300 V and -100 V, the Ar^{13+} production remained largely constant, similar to the inner shell ionization rate. This leads to the conclusion that the bulk of the cold electrons is reflected with

a biased disc voltage $\leq$ -100 V. By therefore increasing the negative bias voltage beyond -100 V, the electron reflection is not significantly enhanced which implies that the warm electron population remains largely constant. This results in both the Ar^{13+} production and the absolute inner shell ionization rate remaining largely unperturbed as observed with this investigation. From the literature it is known that the typical energy of the cold electron population is approximately 50 eV[26]. This further strengthens the argument that the cold electron reflection should saturate with negative biased disc voltage beyond $\sim$-50 V. The investigation also reveals that the inner shell ionization rate peaks at -50 V, while the maximum Ar^{13+} Faraday cup current is observed at -100 V. From -100 V to -20 V, the Ar^{13+} production decreases drastically from 6.4 eμA to 0.37 eμA. During the same voltage interval, the inner shell ionization rate only decreases by 14%. The fact that the absolute inner shell ionization rate does not directly follow the Ar^{13+} production leads to the suggestion that the ionization degree of the plasma decreases as the negative biased disc voltage is decreased from -100 V to -20 V. This is also evident from the mean extracted charge state as a function of the voltage sweep. As the biased disc voltage is decreased from -100 V to -20 V, the mean extracted charge state distribution decreases drastically. The fact that the biased disc voltage does not affect the volumetric emission rate, but affects the CSD implies that optimizing the biased disc voltage affects the confinement time of the ions. The last observation that can be drawn from the current investigation is that the secondary electron emission from the biased disc appears not to account for its performance. The results of this investigation clearly show that the thick-target counts from the biased disc remain largely unperturbed during the voltage sweep. This would result in constant secondary electron emission from the biased disc. The secondary electron emission, from the biased disc, therefore appears to be decoupled from high charge state production.

. From the behaviour of the inner shell ionization rate as a function of the magnetic field strength and biased disc voltage it can be observed that the

inner shell ionization rate remains largely constant, within the experimental uncertainty, during the parameter sweeps. In stark contrast to this, the beam currents of low and high charge states can change drastically over the course of the parameter sweeps. This highlights the fact that the changes in the plasma behaviour, induced during the parameter sweeps manifests differently in the $K\alpha$ emission rate and the extracted ion beam currents of the different charge states. This underlines the importance of using $K\alpha$ emission as a plasma diagnostic and benchmarking tool for ECRIS simulations.

4.3. Comparison of the JYFL 14 GHz ECRIS and GTS at iThemba LABS in terms of absolute inner shell ionization rate

. To confirm that the absolute inner shell ionization rates measured with the JYFL 14 GHz ECRIS are valid, at least to within an order of magnitude, it was necessary to measure and compare the $K\alpha$ emission rates from two different sources. For this comparison, the volumetric $K\alpha$ emission rate of argon was measured from the two ion sources, as a function of the source tune parameters. Figure 13a shows the total absolute inner shell ionization rate for the two ion sources, as a function of absorbed microwave power. The ion source settings for the GTS, during the parametric sweep, were very similar to those of the JYFL 14 GHz ECRIS and represent typical operating conditions used for ion beam production. From the results of the microwave power sweep it can be observed that the absolute inner shell ionization rate of the GTS is very similar to that of the JYFL 14 GHz ECRIS. The general trend is also the same for both sources, i.e. the ionization rate increases with increasing microwave power. The propagated error on the absolute inner shell ionization rate of the GTS is roughly half of that of the JYFL 14 GHz ECRIS, due to the smaller error in the alignment of the position of the X-ray detector in the case of the measurements performed on the GTS. With the pressure sweep, the order of magnitude of the inner shell ionization rate again matches well when the sources are compared. Figure 13b presents the absolute inner shell ionization rate of the JYFL 14 GHz ECRIS as a function of neutral gas pressure, at 400 W of incident microwave power, at

two different times during the measurement period. The absolute inner shell ionization rate measured with the GTS at roughly the same source settings varies between $1.50 \times 10^{10}\text{cm}^{-3}\text{s}^{-1}$ and $1.27 \times 10^{11}\text{cm}^{-3}\text{s}^{-1}$. This comparison is however subject to some uncertainty. Due to the different locations of the pressure gauge and the different pumping speeds, it is difficult to estimate the pressure. The location of the pressure gauge is also different in the case of the GTS at iThemba LABS as oppose to the JYFL 14 GHz ECRIS. The actual pressures in the chamber are therefore probably different for the curves shown in figure 13b compared to the pressures used for the measurements on the GTS. Additionally in the case of the measurements performed with the GTS, the neutral pressure at injection were not determined without microwave power. With microwave power launched into the plasma chamber, the ECR volume acts as a neutral gas sink resulting in a pressure drop in the region of the pressure gauge. This therefore results in a pressure difference with and without microwave power. With the pressure sweep on the GTS, the valve controlling the amount of gas flow to the source injection region was adjusted to three different values, yielding high, medium and low flow rates. These were then compared to typical high, medium and low flow rates of the JYFL 14 GHz ECRIS. The general behaviour of the two sources during the pressure sweep were similar. The trend observed was for the inner shell ionization rate to increase with increasing neutral pressure. For the magnetic field configuration and the biased disc voltage the dependencies were very similar.

5. Conclusions

. The influence of the ECRIS tune parameters on the absolute inner shell ionization rate was studied with two different ion sources. By combining the absolute inner shell ionization rate with the extracted charge state distribution, the study enabled a deeper understanding of high charge state production. Taking into consideration the propagated error as a result of the major uncertainties in the experimental arrangement and atomic processes, the absolute inner shell ioniza-

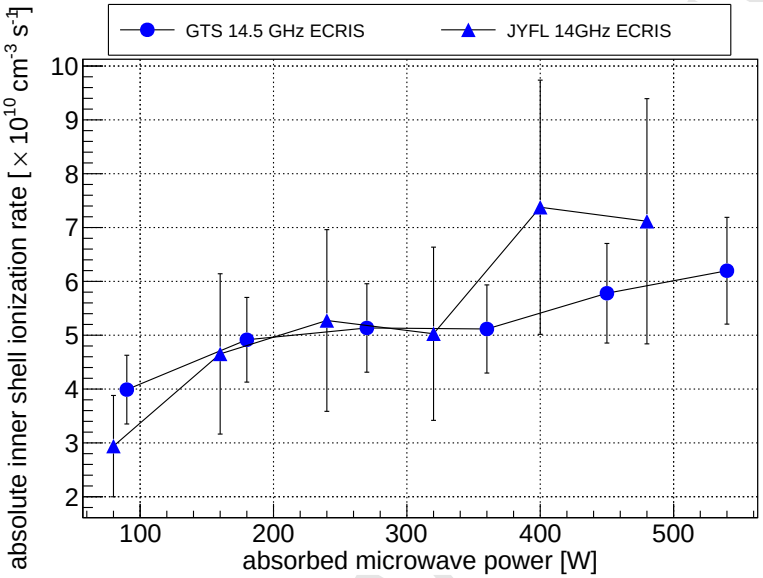

(a) Comparison of the (minimum) absolute inner shell ionization rates. Variation of the (minimum) absolute inner shell ionization rate as a function of absorbed microwave power for the two ECR ion sources.

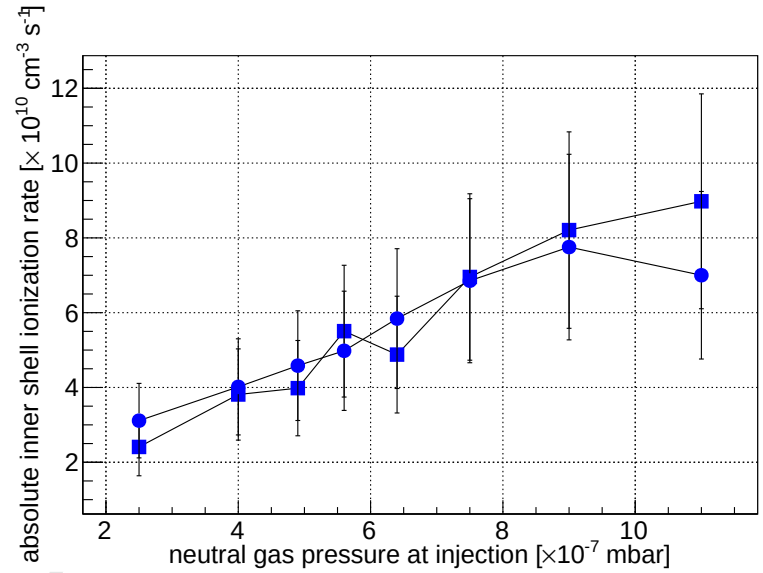

(b) Comparison of the (minimum) absolute inner shell ionization rates. Variation of the (minimum) absolute inner shell ionization rate of the JYFL 14 GHz ECRIS as a function of neutral gas pressure at 400 W of incident microwave power. The inner shell ionization rate was determine at two different times during the measurement period at the same source settings.

Figure 13: Comparison of the (minimum) absolute inner shell ionization rates.

tion rate determined from the two ion sources were very similar. The microwave power and neutral gas pressure were found to have the largest impact on the absolute inner shell ionization rate. The increase in inner shell ionization rate, with increasing microwave power, was found to most likely occur as a result of the increasing plasma energy content. The plasma energy content was also found to saturate as the absorbed microwave power is increased. This leads to the suggestion of a logarithmic increase of $K\alpha$ emission with increasing microwave power. The investigation also revealed that the inner shell ionization rate at low degree of ionization is largely controlled by the target (atom and ion) densities as oppose to the plasma energy content. The influence of the neutral gas pressure on the inner shell ionization rate was found to be larger than the microwave power sweep. This rapid increase was found to be driven by the target densities and the plasma energy content. It was also established that the plasma energy content beyond a certain neutral gas pressure becomes insufficient to sustain the growth in inner shell ionization rate. Above this critical point, the absolute inner shell ionization rate saturates. With further increase in neutral gas pressure, charge exchange processes became dominant resulting in decreased high charge state currents.

. The results of the investigation also showed that the influence of the magnetic field and the biased disc voltage on the inner shell ionization rate was far less pronounced, when compared to the microwave power and neutral pressure sweeps. This led to the suggestion that the magnetic field and the bias disc voltage do not directly affect the warm electron population but influences inner shell ionization via indirect avenues. The influence of the bias disc voltage was attributed to the increasing cold electron reflection. The investigation also concluded that secondary electron emission plays a minimal role. The influence of the axial ion losses was not adequately investigated with this study and will perhaps be probed with a future investigation. The magnetic field configuration was studied using a novel parameter to characterize the influence of the magnetic field variation on the absolute inner shell ionization rate. Using

the average parallel magnetic field gradient over the entire ECR surface, the inner shell ionization was found to be largely decoupled from this parameter. Combining the results of the current investigation with an investigation on the plasma bremsstrahlung, it was concluded that the magnetic field variation acts largely on the hot electron population[38]. It has been suggested that the magnetic field gradient results in heating of warm electrons to hot electrons[11]. The results of the current investigation indicates that the source performance is slightly improved, up to a certain point, by decreasing the average magnetic field gradient.

. The plasma diagnostic developed with this work will be used in future experiments to gain a better understanding of the gas mixing effect and the double frequency heating mechanisms. The beneficial influence of both processes have been abundantly demonstrated with routine operation on various ion sources, yet the detailed understanding of these processes remains not well understood. By mixing two gases one could study the influence of the rate coefficient on the absolute inner shell ionization rate and exclude the influence of the electron density. By then varying any of the source tune parameters, one could study how this changes the absolute inner shell ionization rate. The latter effect as an example is said to alter the excited mode patterns over the ECR surface. By combining frequency tuning with the current diagnostic the current understanding wave-plasma energy transfer could be enhanced.

Acknowledgments

. MS wishes to thank Prof. Paul Papka and the Department of Physics at the University of Stellenbosch for the use of their Silicon Drift Detector (X123-SDD) during the work described in this manuscript. The work of OT has been supported by the Väisälä Foundation of the Finnish Academy of Science and Letters. This research was conducted at JYFL and iThemba LABS and MS wishes to thank all those involved for their support. This work has been supported by the Academy of Finland under the Finnish Center of Excellence

Program (Contract No. 213503) and mobility grant (No. 290390). The work is also based on the research supported in part by iThemba LABS and the National Research Foundation of South Africa (Grant No. 90741).

References

[1] R. Geller, Electron Cyclotron Resonance Ion Sources and ECR Plasmas, 1st Edition, Institute of Physics Publishing, Bristol, 1996.

[2] W. Bambynek, B. Crasemann, R. Fink, et al., X-ray fluorescence yields, auger, and coster kronig transition probabilities, Reviews of modern physics 44 (4) (1972) 716–813. doi:https://doi.org/10.1103/RevModPhys.44.716.

[3] M. Krause, Atomic radiative and radiationless yields for k and l shells, Journal of Physical and Chemical Reference Data 8 (2) (1979) 307–327. doi:http://dx.doi.org/10.1063/1.555594.

[4] P. Auger, The compound photoelectric effect, Journal de Physique et le Radium 6 (6) (1925) 205–208. doi:10.1051/jphysrad:0192500606020500.

[5] D. Coster, R. Kronig, New type of auger effect and its influence on the x-ray spectrum, Physica 2 (1) (1935) 13–24. doi:10.1016/S0031-8914(35)90060-X.

[6] H. Koivisto, P. Heikkinen, V. Hänninen, A. Lassila, H. Leinonen, V. Nieminen, J. Pakarinen, K. Ranttila, J. Ärje, E. Liukkonen, The first results with the new jyfl 14 ghz ecr ion source, Nuclear Instruments and Methods in Physics Research B 174 (3) (2001) 379–384. doi:10.1016/S0168-583X(00)00615-7.

[7] D. Hitz, D. Cormer, J. Mathonnet, A new room temperature ecr ion source for accelerator facilities, Proceeding of EPAC (2002) 1718–1720.

[8] D. Hitz, A. Girard, K. Serebrennikov, G. G. Melin, D. Cormier, J. Mathonnet, J. Chartier, Production of highly charged ion beams with the grenoble test electron cyclotron resonance ion source, Review of Scientic Instruments 75 (5) (2004) 1403–1406. doi:http://dx.doi.org/10.1063/1.1675930.

[9] Amptek website [cited 21 December 2015].
URL http://www.amptek.com

[10] J. Vámosi, S. Biri, Trapcad - a tool to design and study magnetic traps of ecr ion sources, Nuclear Instruments and Methods in Physics Research B 94 (3) (1994) 297–305. doi:10.1016/0168-583X(94)95369-4.

[11] D. Mascali, A new approach to the study of the ecr heating and particle dynamics in the plasma of electron cyclotron resonance ion sources, PhD dissertation, Università Degli Studi Di Catania (2008).

[12] V. V. Mironov, J. Beijers, Three-dimensional simulations of ion dynamics in the plasma of an electron cyclotron resonance ion source, Physical Review Special Topics - Accelerators and Beams 12 (7) (2009) 073501–1. doi:10.1103/PhysRevSTAB.12.073501.

[13] G. Shirkov, T. Nakagawa, Numerical simulation of highly charged ion production in riken 18 ghz electron cyclotron resonance ion source, Review of Scientific Instruments 69 (2) (2009) 1141–1143. doi:10.1063/1.1148649.

[14] Kobra3d-inp, inp.
URL www.inp-dme.com

[15] D. Edgell, J. Kim, I. Bogatu, R. Vondrasek, Modelling of electron cyclotron resonance ion source plasmas, Proceedings of the Particle Accelerator Conference (2001) 2135–2137.

[16] K. Bernhardi, K. Wiesemann, X-ray bremsstrahlung measurements on an ecr-discharge in a magnetic mirror, Plasma Physics 24 (8) (1982) 867–884. doi:10.1088/0032-1028/24/8/001.

[17] R. Friedlein, G. Zschornack, Angle dispersive de-convolution of bremsstrahlung spectra from plasma, Nuclear Instruments and Methods in Physics Research A 349 (2-3) (1994) 554–557. doi:10.1016/0168-9002(94)91226-2.

[18] M. Lamoreux, P. Charles, General deconvolution of thin-target and thick-target bremsstrahlung spectra to determine electron energy distributions, Radiation Physics and Chemistry 75 (10) (2006) 1220–1231. doi:10.1016/j.radphyschem.2006.06.006.

[19] K. Bernhardi, An improved deconvolution method for bremsstrahlung spectra from hot plasmas, Computer Physics Communications 19 (1) (1980) 17–21. doi:10.1016/0010-4655(80)90061-2.

[20] C. Barué, M. Lamoureux, P. Briand, A. Girard, G. Melin, Investigations of hot electrons in electron-cyclotron-resonance ion sources, Journal of applied physics 76 (5) (1994) 2662–2670. doi:10.1063/1.357563.

[21] H. van Regemorter, Rate of collisional excitation in stellar atmospheres, Astrophysical journal 136 (1962) 906–915. doi:10.1086/147445.

[22] D. Sampson, H. Zhang, Use of the van regemorter formula for collision strengths or cross sections, Physical Review A 45 (1992) 1556–1560.

[23] V. Fisher, et al, Electron-impact excitation cross section of hydrogenlike ions, Physical Review A 55 (1) (1997) 329–334. doi:10.1103/PhysRevA.55.329.

[24] W. Lotz, Electron-impact ionization cross-sections and ionization rate coefficients for atoms and ions from hydrogen to calcium, Zeitschrift für Physik 216 (3) (1968) 241–247. doi:10.1007/BF01392963.

[25] G. Shirkov, C. Mühle, G. Musiol, C. Zschornack, Ionization and charge dispersion in electron cyclotron resonance ion sources, Nuclear Instruments and Methods in Physics Research A 302 (1) (1991) 1–5. doi:10.1016/0168-9002(91)90485-9.

[26] G. Douysset, H. Khodja, A. G. J. Briand, Highly charged ion densities and ion confinement properties in an electron-cyclotron-resonance ion source, Physical Review E 61 (3) (2000) 3015–3022. doi:10.1103/PhysRevE.61.3015.

[27] G. Zschornack, Handbook of X-ray data, 2nd Edition, Springer, Berlin, 2007.

[28] C. Barkla, X-rays and the theory of radiation, Journal of the Röntgen Society 14 (55) (1918) 73. doi:10.1259/jrs.1918.0039.

[29] A. Müller, R. Frode, Scaling of cross sections for multiple electron transfer to highly charged ions colliding with atoms and molecules, Physics Review 44 (1080) 29.

[30] A. Müller, R. Frode, Scaling of cross sections for multiple electron transfer to highly charged ions colliding with atoms and molecules, Physics Letter 59 (1976) 19.

[31] R. Thomae, et al, Beam experiments with the grenoble test electron cyclotron resonance ion source at ithemba labs, Review of Scientic Instruments 87 (2) (2016) 623–625. doi:10.1063/1.4935630.

[32] J. Komppula, O. Tarvainen, T. Kalvas, H. Koivisto, R. Kronholm, J. Laulainen, J. J. Myllyrperkiö, Vuv irradiance measurement of a 2.45 ghz microwave-driven hydrogen discharge, Journal of Physics D: Applied Physics 48 (36) (2015) 1–12. doi:10.1088/0022-3727/48/36/365201.

[33] X-ray attenuation and absorption calculator [cited 31 December 2016]. URL http://web-docs.gsi.de

[34] Root: An object-orientated data analysis framework [cited 15 March 2011]. URL http://root.cern.ch/drupal/

[35] M. Morhac, Multidimensional peak searching algorithm for low-statistics nuclear spectra, Nuclear Instruments Methods A 581 (2007) 821–830.

[36] C. Ryan, E. Clayton, W. Criffin, S. H. S.H. Sie, D. Cousens, A statistics-sensitive background treatment for the quantitative analysis of pixe spectra in geoscience applications,, Nuclear Instruments Methods B 34 (1998) 396.

[37] G. Melin, et al, Some particular aspects of the physics of ecr sources for multiplicharged ions, Review of Scientific Instruments 61 (1) (1990) 236–238. doi:10.1063/1.1141305.

[38] J. Noland, O. Tarvainen, Benitez, D. Leitner, C. Lyneis, Verboncoeur, Studies of electron heating on a 6.4 ghz ecr ion source through measurement of diamagnetic current and plasma bremsstrahlung, Plasma Sources Science and Technology 20 (3) (2011) 1–11. doi:10.1088/0963-0252/20/3/035022.

[39] O. Tarvainen, Studies of electron cyclotron resonance ion source plasma physics, PhD dissertation, University of Jyväskylä (2005).

[40] A. Girard, C. Pernot, G. Melin, J. Lécot, Modeling of electron-cyclotron resonance-heated plasma, Physical Review E 62 (1) (2000) 1182–1189. doi:10.1103/PhysRevE.62.1182.

[41] O. Tarvainen, J. Laulainen, J. Komppula, R. Kronholm, T. Kalvas, H. Koivisto, I. Izovtov, D. Mansfeld, V. Skalyga, Limitations of electron cyclotron resonance ion source performance set by kinetic plasma instabilities, Review of Scientific Instruments 86 (2) (2015) 1–9. doi:10.1063/1.4906804.

[42] T. Ropponen, O. Tarvainen, P. Jones, P. Peura, T. Kalvas, P. Suominen, H. Koivisto, J. Ärje, The effects of magnetic field strength on the time evolution of high energy bremsstrahlung radiation created by an electron cyclotron resonance ion source, Nuclear Instruments and Methods in Physics Research A 600 (3) (2009) 525–533. doi:10.1016/j.nima.2008.12.065.

[43] O. Tarvainen, P. Suominen, H. Koivisto, A new plasma potential measure-

ment instrument for plasma ion sources, Review of Scientific Instruments 75 (10) (2004) 3138–3145. doi:10.1063/1.1790559.

[44] A. Drentje, U. Wolters, A. Nadzeyka, D. Meyer, K. Wiesemann, Simon short circuit effect in ecris, Review of Scientific Instruments 73 (2) (2002) 623–625. doi:10.1063/1.1429315.